Phase separation drives heterochromatin domain formation

Amy R. Strom[1,2], Alexander V. Emelyanov[3], Mustafa Mir[2], Dmitry V. Fyodorov[3], Xavier Darzacq[2] & Gary H. Karpen[1,2]

Constitutive heterochromatin is an important component of eukaryotic genomes that has essential roles in nuclear architecture, DNA repair and genome stability[1], and silencing of transposon and gene expression[2]. Heterochromatin is highly enriched for repetitive sequences, and is defined epigenetically by methylation of histone H3 at lysine 9 and recruitment of its binding partner heterochromatin protein 1 (HP1). A prevalent view of heterochromatic silencing is that these and associated factors lead to chromatin compaction, resulting in steric exclusion of regulatory proteins such as RNA polymerase from the underlying DNA[3]. However, compaction alone does not account for the formation of distinct, multi-chromosomal, membrane-less heterochromatin domains within the nucleus, fast diffusion of proteins inside the domain, and other dynamic features of heterochromatin. Here we present data that support an alternative hypothesis: that the formation of heterochromatin domains is mediated by phase separation, a phenomenon that gives rise to diverse non-membrane-bound nuclear, cytoplasmic and extracellular compartments[4]. We show that *Drosophila* HP1a protein undergoes liquid–liquid demixing *in vitro*, and nucleates into foci that display liquid properties during the first stages of heterochromatin domain formation in early *Drosophila* embryos. Furthermore, in both *Drosophila* and mammalian cells, heterochromatin domains exhibit dynamics that are characteristic of liquid phase-separation, including sensitivity to the disruption of weak hydrophobic interactions, and reduced diffusion, increased coordinated movement and inert probe exclusion at the domain boundary. We conclude that heterochromatic domains form via phase separation, and mature into a structure that includes liquid and stable compartments. We propose that emergent biophysical properties associated with phase-separated systems are critical to understanding the unusual behaviours of heterochromatin, and how chromatin domains in general regulate essential nuclear functions.

Proteins that undergo liquid–liquid demixing *in vitro* and *in vivo* often contain intrinsically disordered regions (IDRs) and/or low-complexity sequences[5], which are present in the N-terminal tail and hinge domains of *Drosophila* HP1a (Extended Data Fig. 1a). We therefore expressed and purified *Drosophila* HP1a protein from *Escherichia coli* to determine whether it undergoes phase separation *in vitro*. At 22 °C, high protein concentrations and low levels of salt, aqueous solutions of HP1a spontaneously demixed to form droplets (Fig. 1a, b) that reversibly dissolved at 37 °C (Extended Data Fig. 1b), as observed for other phase-separating proteins[6–8]. These droplets are highly spherical and their area distribution fits a power law with exponent −1.5, suggesting that they are liquid-like and undergo coarsening[9] (Extended Data Fig. 1c, d). Large oligomeric complexes of purified HP1a also formed in glycerol gradients in low but not high salt conditions (Extended Data Fig. 1e, f). Independently, Larson *et al.*[10] report that human HP1α protein (also known as CBX5) also displays liquid demixing *in vitro*, demonstrating a conserved property of diverged HP1 proteins. In contrast to our observations with *Drosophila* HP1a, human HP1α

demixing requires N-terminal phosphorylation or DNA binding, which could be a result of differences in species-specific amino acid sequences or *in vitro* conditions.

To determine the *in vivo* relevance of HP1a demixing, we analysed the first stages of heterochromatin formation in early *Drosophila*
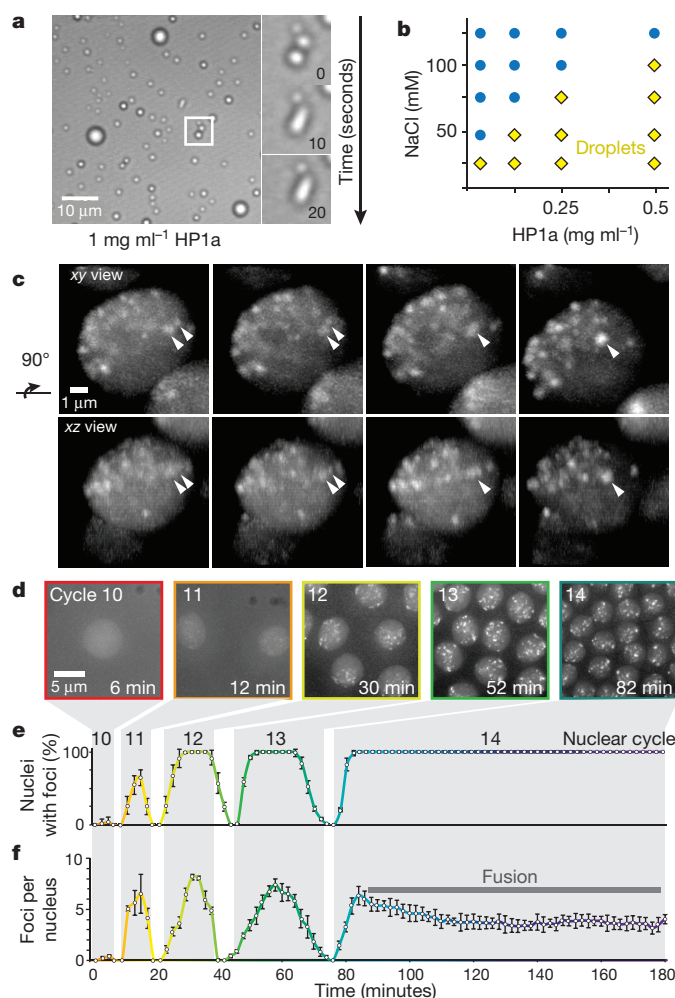
Figure 1 | HP1a exhibits liquid demixing *in vitro* and *in vivo*. a, Purified *Drosophila* HP1a forms liquid phase droplets *in vitro* that undergo fusion. **b**, Phase diagram of HP1a droplet formation at indicated salt and protein concentrations. **c**, In nuclei of *Drosophila* embryos, GFP–HP1a forms liquid droplets that fuse and round up. **d**, HP1a droplets form in every interphase after nuclear cycle 11. **e**, Quantification of average per cent of nuclei with HP1a foci in cycles 10–14. **f**, Quantification of average number of HP1a foci per nucleus in cycles 10–14. Error bars in **e** and **f** are s.d. $n = 12$ embryos of >75 nuclei each.

[1]Biological Systems and Engineering Division, Lawrence Berkeley National Laboratory, Berkeley, California, USA. [2]Department of Molecular and Cell Biology, University of California, Berkeley, California, USA. [3]Albert Einstein College of Medicine, Department of Cell Biology, New York, New York, USA.

embryos. Heterochromatin begins to form during the short (approximately 8–20 min) post-fertilization nuclear cycles 11–13, but does not mature into a stable domain until cycle 14, when interphase extends to 1.5 h (ref. 11). In each of these cycles, we observe that GFP–HP1a exhibits the nucleation, growth and fusion dynamics associated with phase-separated, liquid compartments[4,12]. High-resolution 4D analysis using lattice light-sheet microscopy[13] revealed that HP1a is initially diffuse, then forms highly spherical foci that grow, frequently fuse together, and dissolve at the onset of mitotic prophase, when HP1a is removed from chromatin[14] (Fig. 1c, Supplementary Videos 1–3). Wide-field microscopy shows that in nuclear cycles 11–14, 6–8 HP1a major foci appear simultaneously in early interphase (Fig. 1d–f), grow in cross-section at a rate of 0.45 μm² per min (Extended Data Fig. 1h), and dissolve during mitosis (Extended Data Fig. 1g). Importantly, the total fluorescence intensity of GFP–HP1a does not change during cycles 10–14 (Extended Data Fig. 1i), suggesting that formation and dissolution of HP1a foci is not controlled by changes in protein concentration.

Fusion of droplets to form larger, spherical compartments is a property of liquids[12]. In cycle 13 and early cycle 14 embryos, HP1a foci round up and remain circular (in 2D) after fusion, but display lower circularity as cycle 14 progresses (Fig. 2a, c, Supplementary Videos 1–3). Notably, mature heterochromatin domains appear roughly spherical in some eukaryotic cell types, such as early *Drosophila* embryos, but are aspherical in other cell types (Extended Data Fig. 1j). To assess whether loss of circularity reflects reduced liquid-like behaviour, we used fluorescence recovery after photobleaching (FRAP) to measure the mobile and immobile HP1a fractions during cycles 10–14, and after gastrulation (stage 8). The immobile fraction was undetectable in cycle 10, rose to around 2.5–10% in cycles 11–13 and early cycle 14, and peaked at approximately 30% in late cycle 14 (Fig. 2b), equivalent to stage 8 embryos (Extended Data Fig. 2a, b). Thus, loss of circularity is accompanied by a significant increase in the HP1a immobile fraction, which we speculate is a result of more HP1a associating with the chromatin polymer, whose inherent elasticity introduces shape constraints[15].

Formation of compartments by phase separation often requires weak hydrophobic interactions among macromolecules, which can account for phase components displaying both high concentrations and high mobility[4]. Therefore, we analysed the response of *in vivo* heterochromatin domains to 1,6-hexanediol, an aliphatic alcohol that specifically disrupts weak hydrophobic interactions[16]. Addition of 1,6-hexanediol to *Drosophila* S2 and mouse NIH3T3 cultured cells for two minutes resulted in significant but incomplete dispersal of HP1 from the heterochromatic domains; further, HP1 enrichment in domains partially recovered after 1,6-hexanediol removal (Fig. 2d, e). Notably, proposed roles for HP1 in compacting chromatin[17] predict that HP1a dispersal would decrease histone density in heterochromatin; however, hexanediol treatment did not change histone enrichment, probably owing to nuclear dehydration and a decrease in total nuclear size (Extended Data Fig. 2c).

We hypothesized that the HP1 population that is not dispersed by 1,6-hexanediol corresponds to the immobile component observed with FRAP. Consistent with this idea, the immobile fraction of HP1a in S2 cells as determined by FRAP analysis (50%) is similar to the 46% that remains after hexanediol treatment (Fig. 2g, Extended Data Fig. 2d). GFP–HP1a proteins containing point mutations known to disrupt dimerization (I191E) or non-histone partner binding (W200A)[18] displayed significantly increased mobility compared to GFP–HP1a wild-type controls (Extended Data Fig. 2d), and the mutant proteins were nearly completely extracted from the domain by 1,6-hexanediol treatment (Fig. 2f, g). We conclude that the integrity of mature heterochromatin domains relies on weak hydrophobic interactions, and that dimerization and interactions with non-histone binding partners contribute to HP1a immobilization. This is consistent with evidence that networks of multivalent interactions promote demixing *in vitro* and *in vivo*[7,19]. We propose that mature heterochromatic domains consist
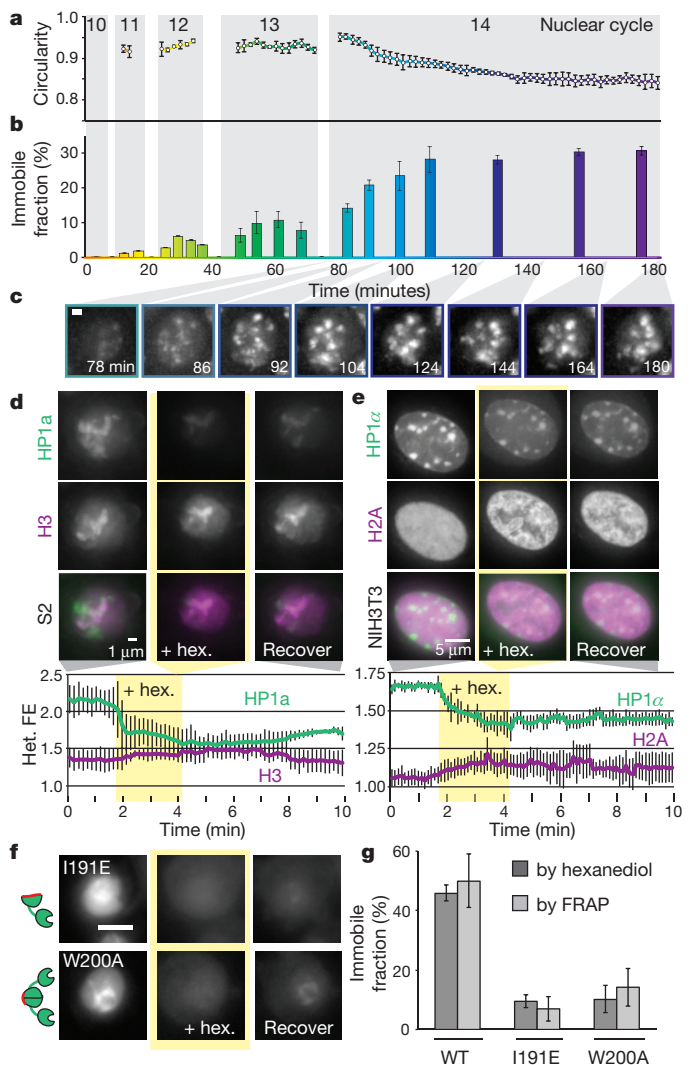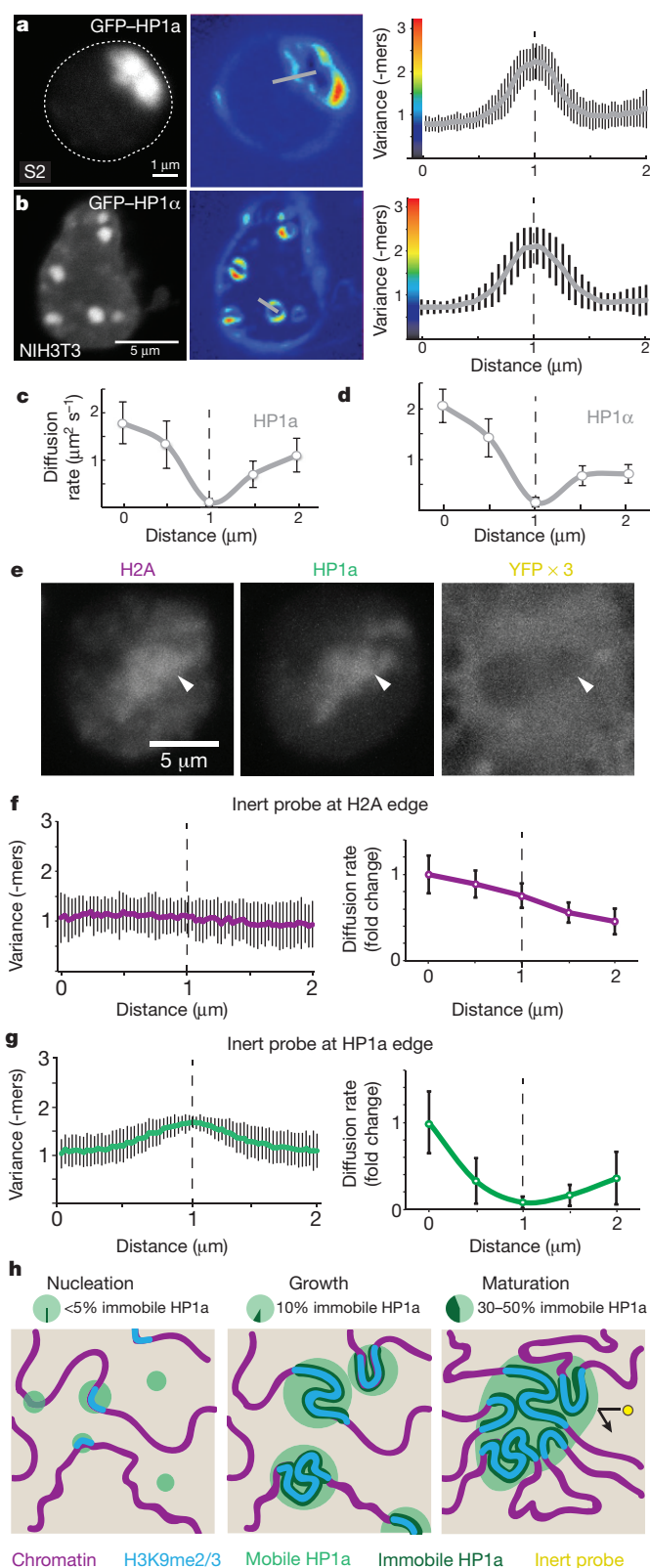

Figure 2 | Mature HP1 domains *in vivo* are not purely liquid.
a, Quantification of average HP1a droplet circularity over cycles 10–14. **b**, Average immobile component of GFP–HP1a measured by FRAP. *n* = 12 embryos, >75 nuclei each, error bars are s.d. **c**, Representative images of HP1a foci during cycle 14. **d, e**, Images and quantification of heterochromatic fold enrichment (FE) of HP1a/α (green) in S2 cells (**d**, *n* = 136 nuclei), or NIH3T3 cells (**e**, *n* = 87 nuclei), treated with 10% 1,6-hexanediol (hex.). Error bars are s.d. Histones (H3/H2A) are shown in magenta. **f**, Representative images of indicated HP1a mutants upon exposure to 1,6-hexanediol. **g**, Immobile fraction of total population for wild type (WT) and mutant HP1a in S2 cells.

of both immobile (static) and mobile (liquid) HP1a compartments, similar to recent findings for nucleoli[20].

To further test the idea that distinct heterochromatin domains arise through phase separation, we analysed HP1a dynamics within and outside these domains in more detail. Macromolecules that self-interact to promote demixing remain spatially confined because free energy must be expended to leave the phase. The magnitude of this free energy cost defines the interfacial tension, and also constrains the directionality of a molecule's movement, increasing the likelihood that two molecules near the phase boundary will move in the same direction ('cooperative' or 'coordinated' movement[21], Extended Data Fig. 3a). Subcellular regions in which fluorescently tagged proteins undergo coordinated movement can be identified by observing increased fluorescence intensity variance using a fluctuation correlation spectroscopy derivative called number and brightness[22] (N&B, Extended Data Fig. 3b). We validated this application of N&B in *Drosophila* S2 cells by first

Figure 3 | The heterochromatin–euchromatin border is a barrier to protein diffusion. a, **b**, Left, fluorescence images of *Drosophila* HP1a (**a**) and mammalian HP1α (**b**); middle, pseudocolour image representing HP1a/α variance; right, quantification of variance across heterochromatin–euchromatin border; dotted line represents domain boundary. $n = 25$ nuclei each, error bars are s.d. **c**, **d**, Average diffusion rate of HP1a (**c**) and HP1α (**d**) across the heterochromatin–euchromatin boundary. $n = 25$ nuclei each, error bars are s.d. **e**, Nucleus expressing mCherry–H2A, Cerulean–HP1a, and NLS–YFP–YFP–YFP as an inert probe excluded from heterochromatin (arrowhead). **f**, **g**, Variance and diffusion rate of inert probe at the edge of H2A-rich domains (**f**) and HP1a-rich domains (**g**). $n = 47$ nuclei each, error bars are s.d. **h**, Model of heterochromatin formation.

High variance at the heterochromatin boundary was also observed for two other heterochromatin proteins, HP4 and HP5 (Extended Data Fig. 3d, e), and for human HP1α (CBX5) and HP1γ (CBX3) expressed in mouse NIH3T3 cells (Fig. 3b, Extended Data Fig. 3f), similar to previous results in mammalian cells[17]. By contrast, HP1c, which is closely related to HP1a but enriched in euchromatin, did not show increased variance near the euchromatin–heterochromatin border (Extended Data Fig. 3g). Together these data demonstrate that HP1a and other heterochromatic proteins exhibit the coordinated movement predicted to occur at phase interfaces.

Constraints on movement at phase interfaces also predict that diffusion rates will be slower at the boundary compared to inside the domain[21] (Extended Data Fig. 3a). To assess the movement of fluorescently tagged HP1a near the heterochromatin domain boundary, we used raster image correlation spectroscopy (RICS)[24]. Here again we validated the approach by analysing GFP–fibrillarin dynamics in S2 cells, and observed much slower diffusion rates near the inner surface ($D = 0.20 \pm 0.18\,\mu m^2\,s^{-1}$), compared to the interior ($1.78 \pm 0.50\,\mu m^2\,s^{-1}$) or outside ($1.72 \pm 0.77\,\mu m^2\,s^{-1}$) the nucleolus (Extended Data Fig. 3h). Similarly, GFP–HP1a (Fig. 3c) displayed reduced diffusion near heterochromatin domain boundaries ($0.10 \pm 0.07\,\mu m^2\,s^{-1}$), compared to the interior of the heterochromatin domain ($1.09 \pm 0.36\,\mu m^2\,s^{-1}$) or the nucleoplasm ($1.78 \pm 0.45\,\mu m^2\,s^{-1}$). HP4 and HP5 showed similar spatial variation in their dynamics (Extended Data Fig. 3h), and human HP1α shows similar behaviour in NIH3T3 cells (near the boundary, $0.15 \pm 0.08\,\mu m^2\,s^{-1}$; internal, $0.71 \pm 0.18\,\mu m^2\,s^{-1}$; nucleoplasm, $2.05 \pm 0.34\,\mu m^2\,s^{-1}$) (Fig. 3d). Thus, two independent methods reveal that *in vivo* HP1a dynamics in both *Drosophila* and mammalian nuclei are consistent with heterochromatin protein containment within liquid-like, phase-separated compartments.

We next assessed whether HP1a is needed for compartmentalization of heterochromatin *in vivo* by depleting it from cultured *Drosophila* S2 cells and examining the effect on the nuclear distribution of HP4 (ref. 25). After HP1a depletion, GFP–HP4 loses coordinated movement and becomes dispersed throughout the nucleus. This is in contrast to restriction of HP4 to a distinct heterochromatic domain in *bw*-depleted control cells, and in HP1a-depleted cells rescued by transfection with RNA interference-resistant, wild-type HP1a (Extended Data Fig. 3i). We conclude that HP1a is required for heterochromatin domain integrity and compartmentalization, but it is likely that other components and interactions also have important roles.

Inert macromolecular probes such as fluorescent dextrans and some proteins are excluded from heterochromatin[26], which has been attributed to steric exclusion as a consequence of chromatin compaction. To test whether exclusion might instead reflect selective permeability of heterochromatic compartments, we co-expressed an inert probe (NLS–YFP–YFP–YFP, 89 kDa) with mCherry–H2A and Cerulean–HP1a in S2 cells (Fig. 3e–g), and observed variance and diffusion of the inert probe at the boundary of areas of high H2A density or high HP1a density. If phase interactions have greater influence on probe movement than compaction, probe variance and diffusion will be impacted more

analysing nucleoli, which are known to arise through phase separation[23]. N&B analysis of GFP–fibrillarin highlighted areas of consistently high variance (2.38 ± 0.46 -mers) at the nucleolar boundary, compared to inside (1.28 ± 0.36) or outside (1.17 ± 0.25) the domain (Extended Data Fig. 3c). Similarly, GFP–HP1a displayed increased variance near the heterochromatin domain boundary (2.06 ± 0.31), compared to inside (1.23 ± 0.38) or outside (0.95 ± 0.15) the domain (Fig. 3a).

by high HP1a density than high H2A density (Extended Data Fig. 3j). Consistent with the phase model, variance of the probe did not spatially correlate with H2A density, but was elevated at the edges of HP1a-rich domains (1.45 ± 0.09, Fig. 3f, g). We also observed reduced probe diffusion within H2A-dense regions ($45\% \pm 14\%$ of the euchromatic rate), suggesting that chromatin density does hinder movement. However, proximity to the heterochromatin border had a much stronger effect on diffusion rates (0.17 ± 0.12, Fig. 3g). Therefore, we conclude that phase interactions and selective permeability play a dominant role over chromatin compaction in inert probe exclusion from the domain (summarized in Extended Data Fig. 3k).

Based on the combination of *in vivo* and *in vitro* data presented here, we propose a model in which heterochromatin domain formation and behaviours are driven by liquid phase separation, which holistically links emergent properties of the domain to local molecular interactions (Fig. 3h). Some findings, such as the presence of both immobile and mobile HP1 in the domain, are also consistent with canonical HP1–H3K9me2/3 binding models for heterochromatin formation[3]. However, binding is not inconsistent with phase separation, and the liquid behaviours, dependence on weak hydrophobic interactions, and protein dynamics strongly favour the conclusion that heterochromatin domains form via phase separation. We propose that heterochromatin formation begins with nucleation, where all HP1a is mobile and foci begin to form via multivalent, weak hydrophobic interactions between multiple HP1 molecules and other heterochromatin components. Over time these foci undergo growth, during which spherical foci become larger through recruitment of more HP1 and coarsening, and some HP1 becomes immobile. During maturation, foci undergo liquid-like fusion to form larger domains. Loss of circularity of HP1a foci coincides with an increase in immobile, chromatin-bound HP1, resulting in mature domains consisting of both liquid and stable compartments. We propose that the reduced circularity of mature heterochromatin domains is due to the inclusion of significant amounts of the DNA/nucleosome polymer[27], or possibly associations with other nuclear structures (for example, lamina). This contrasts with retention of circularity in phase-separated systems that contain less DNA (for example, nucleoli), or predominantly comprise small, colloidal particles (proteins and RNAs) that are able to freely intermix[4,12,19,28].

The phase-separation model and, in particular, liquid properties of the domain are also attractive theories because they can account for unusual heterochromatin behaviours described in the literature and generate alternative, testable hypotheses about the regulation of heterochromatin functions. For example, associations between distal heterochromatic islands and the main domain[29] is easily accommodated by liquid fusion events that loop the intervening DNA (Extended Data Fig. 3l). Additionally, phase separation provides an alternative to 'mass-action' models to explain the sensitivity of heterochromatin-mediated gene silencing to temperature and heterochromatin protein dosage. The inherent demixing ability of HP1 suggests that nucleation of HP1-rich domains *in vivo* could be independent of chromatin and H3K9me2/3, but it is also possible that this methylation mark is required (Extended Data Fig. 3l). Similarly, HP1-mediated recruitment of H3K9 methyltransferases that modify adjacent nucleosomes is routinely invoked to explain stochastic *cis*-spreading of heterochromatin and gene silencing[3]; however, adjacent sequences (in *cis* or *trans*) could first be engulfed by liquid HP1, followed by histone methyltransferase recruitment and H3K9 methylation (Extended Data Fig. 3l). With respect to regulatory mechanisms, selective permeability imparted by a phase boundary (Extended Data Fig. 3k) provides an alternative mechanism to chromatin compaction for controlling fundamental heterochromatic functions such as transcriptional silencing, replication[30] and prevention of aberrant DNA damage repair[1,2]. We speculate that access to the domain could be regulated by binding a transport protein, similar to nuclear pores and importins[16], or through post-translational modifications. Alternatively, genomic regions could be moved in or out of domains by associating with or disassociating from (respectively)

phase components, as seen for movement of heterochromatic double-strand breaks to outside the domain to complete repair, which is accompanied by local removal of HP1 (ref. 1).

More investigations are needed to elucidate how emergent properties of phase-separated systems affect genome functions, and in particular to identify the features that regulate molecular inclusion or exclusion from the heterochromatic domain. It has been suggested that phase separation is a general organizing principle in cells, so it will be important to determine if other chromatin domains also form and function via phase-separation principles. In sum, these results have led us to a fundamentally different perspective on heterochromatin formation, providing new opportunities for understanding how architectural and biophysical properties influence chromatin domain formation and overall genome function.

Online Content Methods, along with any additional Extended Data display items and Source Data, are available in the online version of the paper; references unique to these sections appear only in the online paper.

1. Chiolo, I. *et al.* Double-strand breaks in heterochromatin move outside of a dynamic HP1a domain to complete recombinational repair. *Cell* **144**, 732–744 (2011).
2. Peng, J. C. & Karpen, G. H. Epigenetic regulation of heterochromatic DNA stability. *Curr. Opin. Genet. Dev.* **18**, 204–211 (2008).
3. Elgin, S. C. R. & Reuter, G. Position-effect variegation, heterochromatin formation, and gene silencing in *Drosophila*. *Cold Spring Harb. Perspect. Biol.* **5**, a017780 (2013).
4. Hyman, A. A., Weber, C. A. & Jülicher, F. Liquid-liquid phase separation in biology. *Annu. Rev. Cell Dev. Biol.* **30**, 39–58 (2014).
5. Kato, M. *et al.* Cell-free formation of RNA granules: low complexity sequence domains form dynamic fibers within hydrogels. *Cell* **149**, 753–767 (2012).
6. Molliex, A. *et al.* Phase separation by low complexity domains promotes stress granule assembly and drives pathological fibrillization. *Cell* **163**, 123–133 (2015).
7. Mitrea, D. M. *et al.* Nucleophosmin integrates within the nucleolus via multi-modal interactions with proteins displaying R-rich linear motifs and rRNA. *eLife* **5**, e13571 (2016).
8. Nott, T. J. *et al.* Phase transition of a disordered nuage protein generates environmentally responsive membraneless organelles. *Mol. Cell* **57**, 936–947 (2015).
9. Huber, G. Scheidegger's rivers, Takayasu's aggregates and continued fractions. *Physica A* **170**, 463–470 (1991).
10. Larson, A. G. *et al.* Reversible liquid droplet formation by HP1α suggests a role for phase separation in heterochromatin. *Nature* http://dx.doi.org/10.1038/nature22822 (2017)
11. Yuan, K. & O'Farrell, P. H. TALE-light imaging reveals maternally guided, H3K9me2/3-independent emergence of functional heterochromatin in *Drosophila* embryos. *Genes Dev.* **30**, 579–593 (2016).
12. Zhu, L. & Brangwynne, C. P. Nuclear bodies: the emerging biophysics of nucleoplasmic phases. *Curr. Opin. Cell Biol.* **34**, 23–30 (2015).
13. Chen, B.-C. *et al.* Lattice light-sheet microscopy: imaging molecules to embryos at high spatiotemporal resolution. *Science* **346**, 1257998 (2014).
14. Fischle, W. *et al.* Regulation of HP1-chromatin binding by histone H3 methylation and phosphorylation. *Nature* **438**, 1116–1122 (2005).
15. Vasquez, P. A. *et al.* Entropy gives rise to topologically associating domains. *Nucleic Acids Res.* **44**, 5540–5549 (2016).
16. Ribbeck, K. & Görlich, D. The permeability barrier of nuclear pore complexes appears to operate via hydrophobic exclusion. *EMBO J.* **21**, 2664–2671 (2002).
17. Hinde, E., Cardarelli, F. & Gratton, E. Spatiotemporal regulation of Heterochromatin Protein 1-alpha oligomerization and dynamics in live cells. *Sci. Rep.* **5**, 12001 (2015).
18. Brower-Toland, B. *et al.* *Drosophila* PIWI associates with chromatin and interacts directly with HP1a. *Genes Dev.* **21**, 2300–2311 (2007).
19. Li, P. *et al.* Phase transitions in the assembly of multivalent signalling proteins. *Nature* **483**, 336–340 (2012).
20. Feric, M. *et al.* Coexisting liquid phases underlie nucleolar subcompartments. *Cell* **165**, 1686–1697 (2016).
21. Hancock, R. & Jeon, K. W. (eds) *New Models of the Cell Nucleus: Crowding, Entropic Forces, Phase Separation, and Fractals.* Vol. 307 (Academic Press, 2013).
22. Digman, M. A., Dalal, R., Horwitz, A. F. & Gratton, E. Mapping the number of molecules and brightness in the laser scanning microscope. *Biophys. J.* **94**, 2320–2332 (2008).
23. Falahati, H., Pelham-Webb, B., Blythe, S. & Wieschaus, E. Nucleation by rRNA dictates the precision of nucleolus assembly. *Curr. Biol.* **26**, 277–285 (2016).
24. Rossow, M. J., Sasaki, J. M., Digman, M. A. & Gratton, E. Raster image correlation spectroscopy in live cells. *Nat. Protocols* **5**, 1761–1774 (2010).

25. Greil, F., de Wit, E., Bussemaker, H. J. & van Steensel, B. HP1 controls genomic targeting of four novel heterochromatin proteins in *Drosophila*. *EMBO J.* **26,** 741–751 (2007).
26. Bancaud, A. *et al.* Molecular crowding affects diffusion and binding of nuclear proteins in heterochromatin and reveals the fractal organization of chromatin. *EMBO J.* **28,** 3785–3798 (2009).
27. Iborra, F. J. Can visco-elastic phase separation, macromolecular crowding and colloidal physics explain nuclear organisation? *Theor. Biol. Med. Model.* **4,** 15 (2007).
28. Brangwynne, C. P., Mitchison, T. J. & Hyman, A. A. Active liquid-like behavior of nucleoli determines their size and shape in *Xenopus laevis* oocytes. *Proc. Natl Acad. Sci. USA* **108,** 4334–4339 (2011).
29. Dernburg, A. F. *et al.* Perturbation of nuclear architecture by long-distance chromosome interactions. *Cell* **85,** 745–759 (1996).
30. Taddei, A., Roche, D., Sibarita, J. B., Turner, B. M. & Almouzni, G. Duplication and maintenance of heterochromatin domains. *J. Cell Biol.* **147,** 1153–1166 (1999).

Supplementary Information is available in the online version of the paper.

METHODS

No statistical methods were used to predetermine sample size. The experiments were not randomized and the investigators were not blinded to allocation during experiments and outcome assessment.

Drosophila embryo imaging. Female *Drosophila* homozygous for GFP–HP1a and RFP–H2Av were crossed to *yw* males and embryos were collected for 2 h, dechorionated, and imaged every 2 min at 60× magnification on a DeltaVision microscope. Images were deconvolved using softWoRx conservative deconvolution, five iterations. Quantification of foci number and circularity were performed with Fiji[31]. Nuclei were identified after smoothing and 12-pixel rolling ball background subtraction by >85% fluorescence intensity thresholding and size >2 μm². HP1a foci were identified after smoothing and 5-pixel rolling ball background subtraction with HP1a threshold >95% fluorescence intensity and size >0.1 μm². Domain size per nucleus, number and circularity measured using the Analyze Particles function in Fiji. Quantifications result from movies of >75 nuclei each in $n = 12$ embryos.

Lattice light-sheet microscopy (LLSM). LLSM was performed on a custom-built implementation of the instrument as previously described[13]. A 30 beam square lattice light sheet, with inner and outer numerical apertures of 0.505 and 0.60 respectively, was generated with a 488 nm input laser and dithered in *x* over a 5 μm range during each exposure to create a uniform excitation sheet. *Z*-stacks were collected by synchronously scanning the excitation sheet and detection objective over a 25 μm range in 250-nm steps. The exposure time for each slice in the stack was 10 ms, and the time interval between stacks was 2.025 s. The laser power was measured to be approximately 700 μW at the back aperture. Data were rendered and analysed using Amira (FEI).

Fluorescence recovery after photobleaching (FRAP). Embryos (prepared as above) were imaged every 2 s for 30 frames at 100× on a DeltaVision microscope. Three images were pre-bleach, and on the fourth approximately 3 μm² was bleached with the 488 nm laser of the quantifiable laser module (QLM). FRAP in S2 cells was performed on selected regions of interest (2 μm²) using a spinning disk confocal (3i) with 100% power and recovery observed at 2% power, 0.5 s intervals for 30 s. Recovery was measured as fluorescence intensity of photobleached area normalized to the intensity of the unbleached heterochromatic area. Immobile fractions 'using FRAP' were measured as per cent fluorescence intensity unrecovered after 30 s.

Hexanediol treatments. Cultured *Drosophila* S2 cells from the *Drosophila* Genomics Resource Center in Schneiders Medium (Sigma-Aldrich S0146) stably expressing GFP-tagged wild-type HP1a, HP1a(I191E), or HP1a(W200A) (in addition to endogenous untagged HP1a) were visualized on a DeltaVision microscope every 5 s for 10 min. At approximately 2 min, normal medium was removed and Schneiders Medium containing 10% 1,6-hexanediol (Sigma-Aldrich 240117-50G) by weight was added. After 2 min more, medium containing hexanediol was removed and replaced with normal Schneiders Medium and recovery was observed for 6 min. Image analysis was performed with Fiji. Nuclei were identified after smoothing and 12-pixel rolling ball background subtraction with a >85% H3 fluorescence intensity threshold. This nuclear area was used to calculate nuclear size. The heterochromatin region was identified after smoothing and 3-pixel rolling ball background subtraction with a threshold of >97.5% HP1a fluorescence intensity. Heterochromatic enrichment was calculated by dividing average intensity of the heterochromatic domain in one nucleus by the average intensity of an equally sized region elsewhere in the same nucleus. Immobile fractions measured 'using hexanediol' were calculated as per cent heterochromatic enrichment remaining after hexanediol treatment for 120 s.

Mammalian cell culture. NIH3T3 cells were obtained as a gift from M. Bissell, and cultured in DMEM containing 10% FBS.

Number and brightness (N&B) and raster image correlation spectroscopy (RICS). Twenty-five consecutive 256 × 256 pixel images were collected at 16 bit depth with pixel dwell time 6.3 μs and 1 AU using a 63× objective with 10× zoom on a Zeiss LSM710 confocal microscope. Images were analysed using SimFCS[22,24,32]. Variance was quantified by measuring individual pixel variance values across a line crossing the domain edge, from outside to inside the domain. At least 10 lines per nucleus were measured, and values from 25 nuclei averaged.

Inert probe properties. Cultured *Drosophila* S2 cells were transiently transfected with CFP–HP1a, mCherry–H2A and YFP–YFP–YFP–NLS, each expressed from a Copia promoter. Nuclei were imaged after 3 days; 25 consecutive 256 × 256 pixel images were collected at 16 bit depth with pixel dwell time 3.1 μs and 1 AU, using a 63× objective with 10× zoom on a Zeiss LSM710 confocal microscope. To calculate average diffusion rate, scan analysis was performed with a 32 × 32 pixel ROI in simFCS at edges of HP1a domains with minimal H2A change (>3 fold intensity increase in HP1a, <1.25 fold intensity increase in H2A), and at edges of H2A-dense domains with minimal HP1a change (>2 fold intensity increase in H2A, <1.25 fold intensity increase in HP1a).

Protein sequence analysis. *Drosophila* HP1a protein amino acid sequence was obtained from FlyBase[33]. Disorder was predicted using Predictor of Natural Disorder Regions (PONDR) version VL-XT[34]. Low complexity sequences were predicted using an online automated segmentation tool (SEG)[35]. Hydrophobicity was predicted using ExPASy[36], using the Kyte and Doolittle scale of amino acid hydropathicity[37].

In vitro droplet assays. Recombinant *Drosophila* Flag–6×His–HP1a was expressed in *E. coli* and purified in three steps by Ni-NTA and anion exchange chromatography (Source 15Q). The purified protein was also subjected to ultracentrifugation (2 h at 260,000*g*) to remove insoluble aggregates. Protein was stored in 25 mM HEPES, pH 7.6, 200 mM NaCl, 0.1 mM EDTA, 10% glycerol, 0.01% NP-40, 1 mM DTT, 0.2 mM PMSF, 0.5 mM benzamidine. Protein was added to 5 μl salt buffer (50 mM HEPES, 5 mM DTT, 25–150 mM NaCl) at 0.05, 0.1, 0.25 and 0.5 mg ml^{-1} in 20-μl PCR tubes, then 1 ml was trapped between two coverslips and imaged with differential interference contrast microscopy at 63× on a Zeiss LSM710 confocal microscope. Images were quantified using Fiji. After smoothing and 5-pixel rolling ball background subtraction, droplets were identified with threshold >99.5% intensity and size >0.1 μm². Aspect ratio calculated for $n = 3$ experiments, each with >300 droplets. Area probability was calculated from movies taken during droplet formation, where coverslips containing 0.5 mg ml^{-1} HP1a in 50 mM NaCl buffer were incubated at 37 °C for 5 min, then returned to 22 °C. Images were taken every 10 s for 8 min to visualize droplet formation. Number and area of droplets were calculated using Fiji with the same specifications as above.

Glycerol gradient sedimentation. Samples of purified recombinant HP1a (2.5 mg ml^{-1}) were incubated for 1 h at 4 °C in buffers containing 50 or 500 mM NaCl and subjected to ultracentrifugation (Beckman SW-41Ti, 41,000 r.p.m., 287,000*g*, 18 h at 4 °C) on linear 10–45% gradients of glycerol in 10 mM HEPES, 1 mM EDTA, 0.01% NP-40, 1 mM DTT, 0.2 mM PMSF, 0.5 mM benzamidine and 50 or 500 mM NaCl. The gradients were cut into 12 fractions and analysed by SDS–PAGE and Coomassie staining.

RNAi experiments. Double-stranded RNA targeting the *bw* gene sequence or the UTR–exon1 junction of HP1a were made from S2 genomic DNA using a MegaScript T7 Transcription Kit. Double-stranded RNA was applied to culture medium on day 1. On day 2, cells were transfected using Mirus Trans-IT 20-20 with GFP–HP4 alone or with an RNAi-resistant mCherry–HP1a. Cells were imaged on day 5 and collected for knockdown validation by western blot.

Data availability statement. The data that support the findings of this study are available from the corresponding author upon request.

31. Schindelin, J. *et al.* Fiji: an open-source platform for biological-image analysis. *Nat. Methods* **9,** 676–682 (2012).
32. Digman, M. A., Wiseman, P. W., Horwitz, A. R. & Gratton, E. Detecting protein complexes in living cells from laser scanning confocal image sequences by the cross correlation raster image spectroscopy method. *Biophys. J.* **96,** 707–716 (2009).
33. Gramates, L. S. *et al.* FlyBase at 25: looking to the future. *Nucleic Acids Res.* **45,** D663–D671 (2017).
34. Romero, P. *et al.* Sequence complexity of disordered protein. *Proteins* **42,** 38–48 (2001).
35. Wootton, J. C. Non-globular domains in protein sequences: automated segmentation using complexity measures. *Comput. Chem.* **18,** 269–285 (1994).
36. Gasteiger, E. *et al.* ExPASy: The proteomics server for in-depth protein knowledge and analysis. *Nucleic Acids Res.* **31,** 3784–3788 (2003).
37. Kyte, J. & Doolittle, R. F. A simple method for displaying the hydropathic character of a protein. *J. Mol. Biol.* **157,** 105–132 (1982).
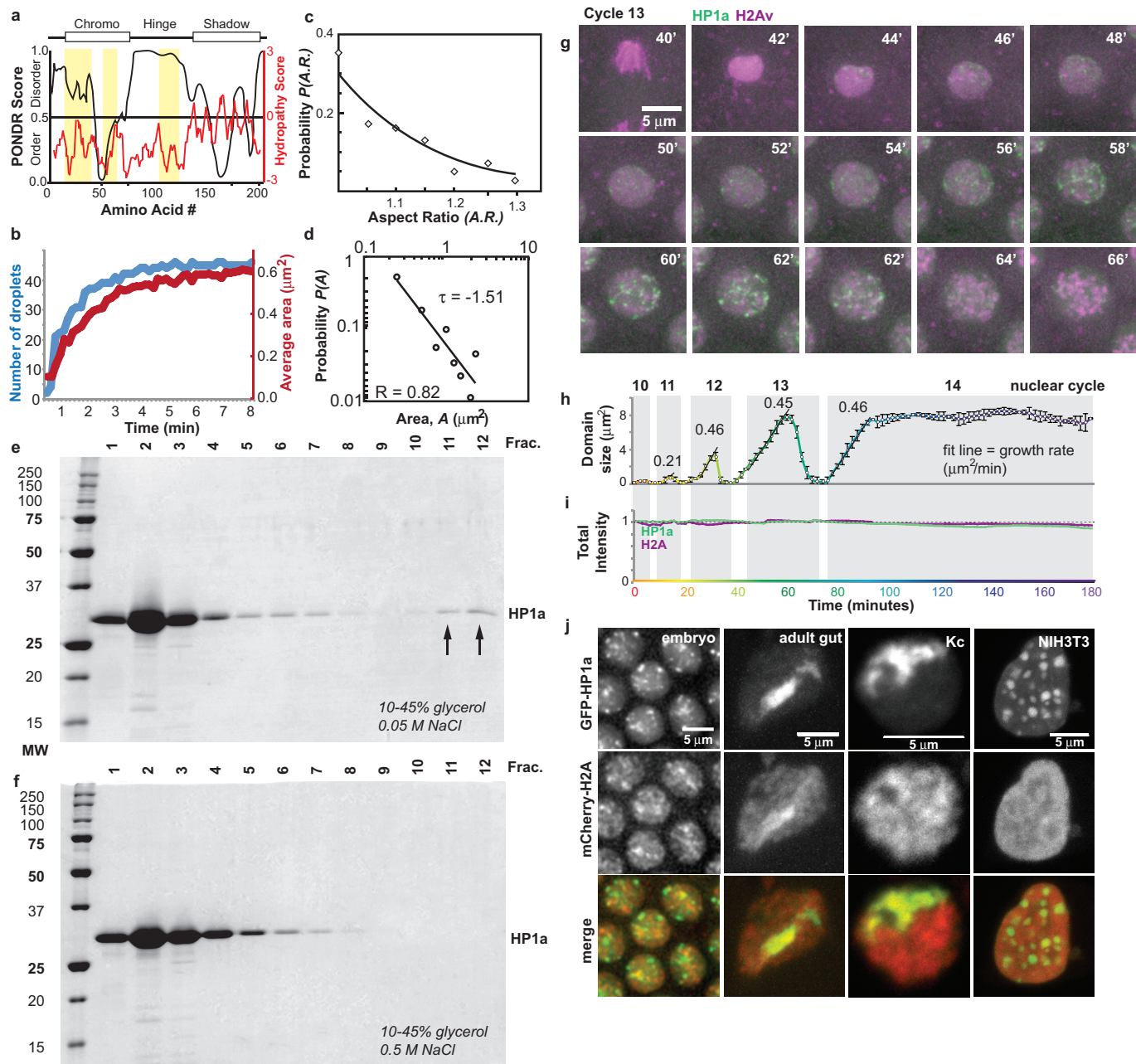
Extended Data Figure 1 | HP1a facilitates liquid demixing *in vitro* and *in vivo*. a, Analysis of HP1a 206 amino acid protein sequence. Top, known domains chromo, hinge, and shadow. Black line, predictor of natural disordered regions (PONDR) score for intrinsic disorder, >0.5 is considered disordered. Red line, hydropathy score (positive is hydrophobic). Yellow bars indicate low-complexity sequences. **b**, 1 mg ml^{-1} HP1a in 50 mM NaCl was incubated at 37 °C for 5 min, then returned to room temperature (22 °C) and imaged with differential interference contrast microscopy (DIC) every 5 s for 8 min. Quantification of average number and area of HP1a droplets formed in a 50 × 50 µm window, $n = 3$. **c**, Probability distribution of droplet aspect ratio. **d**, Probability distribution of droplet area on a log–log plot follows a power

law exponential with $\tau = -1.5$, characteristic of aggregating systems. **e**, **f**, Sediment gradient analysis shows large oligomers of HP1a in 0.05 M NaCl (arrows, **e**) but not 0.5 M NaCl (**f**). **g**, Two-colour images showing HP1a and H2Av for one nucleus over *Drosophila* embryonic cycle 13. **h**, **i**, Quantification of average HP1a domain size per nucleus (sum of all foci in each nucleus) (**h**) and total intensity of fluorescently-tagged HP1a and H2A (**i**), over embryonic cycles 10–14. Error bars are s.d. $n = 12$ embryos of >75 nuclei each. **j**, Two-colour images of HP1a and H2A showing differentially shaped heterochromatin domains in *Drosophila* embryos, adult gut and cultured Kc cells, and mouse fibroblast NIH3T3 cells.
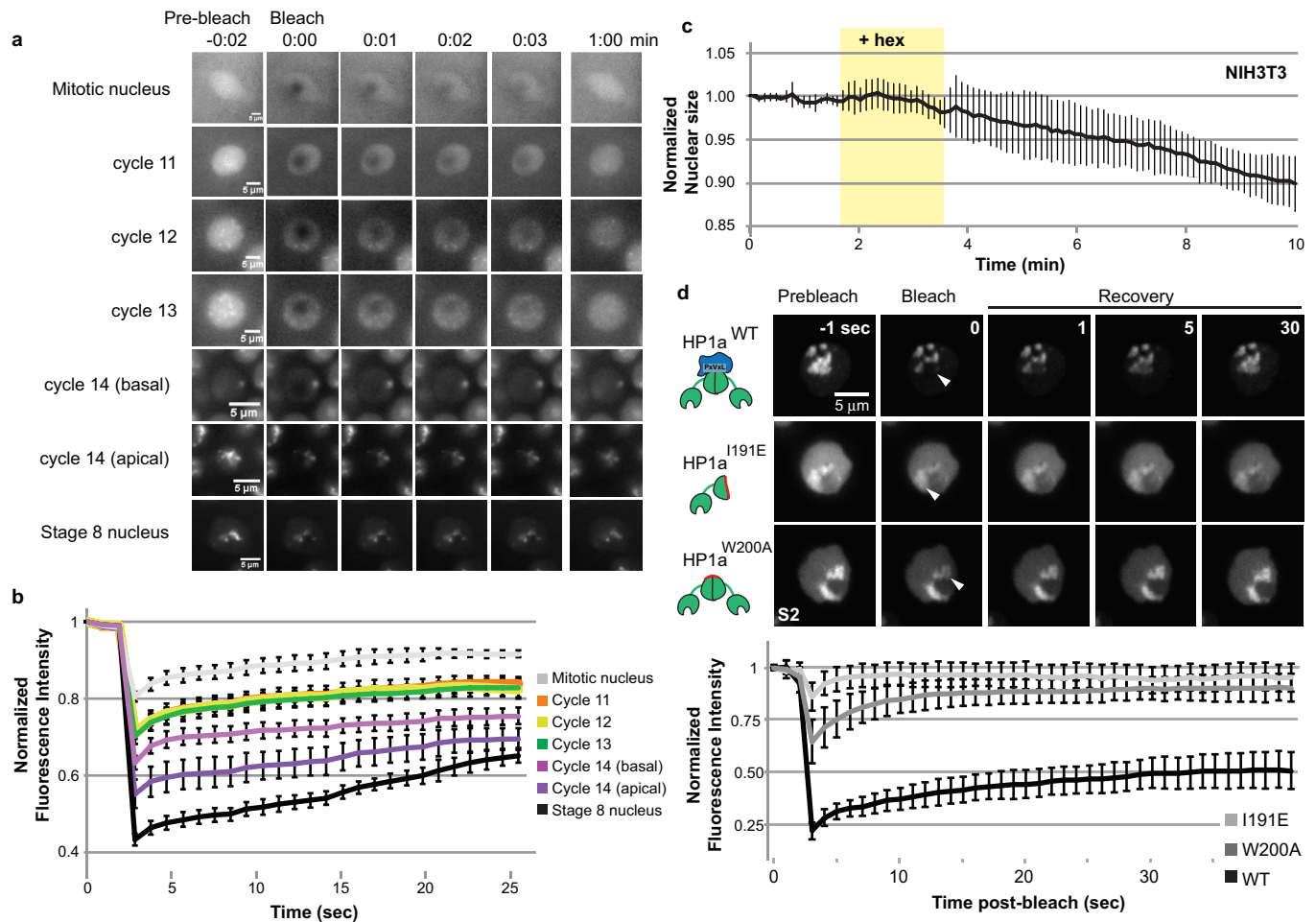
Extended Data Figure 2 | Mature *in vivo* HP1 domains are not pure liquid. a, b, FRAP images (**a**) and average fluorescence intensity over time of bleached area (**b**) of *Drosophila* embryonic nuclei in cycles 10–14, and stage 8. In cycle 14, heterochromatin forms in the apical region of the nucleus. $n = 20$ nuclei in each condition, error bars are s.d. **c,** NIH3T3 nuclear size after addition of media containing 10% 1,6-hexanediol. $n = 63$ nuclei, error bars are s.d. **d,** Images and quantification of FRAP on wild-type (WT) HP1a and point mutants incapable of dimerizing (I191E) or interacting with binding partners (W200A) in S2 cells. $n = 60$ nuclei each condition, error bars are s.d.
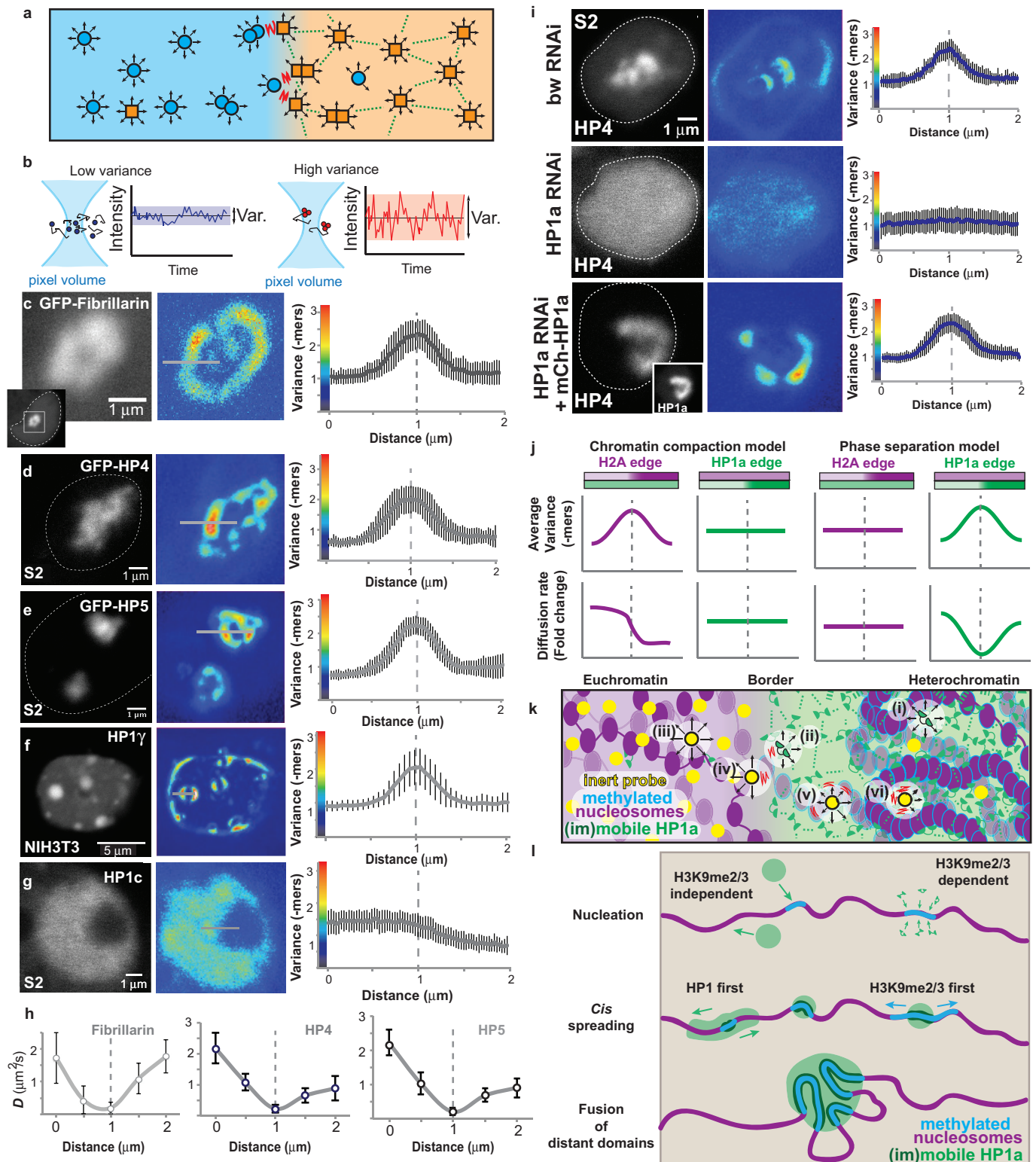
Extended Data Figure 3 | See next page for caption.

Extended Data Figure 3 | The heterochromatin–euchromatin border is a barrier to protein diffusion. a, Schematic illustration of dynamic properties near a phase boundary. Orange particles have self-association properties (green dotted lines) and concentrate into a phase (orange background, right side). An orange particle in the orange phase can move in any direction and encounter only orange particles (eight arrows) until it contacts a blue particle, which prevents self-association between two orange particles and limits the potential diffusion dimensions of the orange particle (red squiggle, loss of arrows). This results in two properties of particles near the phase boundary: net slower diffusion and higher likelihood that two orange particles will move in the same direction. **b**, Schematic illustrating number and brightness technique[22]. If particles are moving independent of one another (left, blue), variations in fluorescence intensity measured in the pixel volume over time will be small. If particles are moving together in and out of the pixel volume (right, red), intensity variation will be larger. This can result from bound molecules (that is, complex) or unbound molecules moving in the same direction (coordinated movement). **c**, A cultured *Drosophila* S2 cell expressing GFP-tagged fibrillarin to mark the nucleolus (left). Inset shows entire nucleus (dotted line) and region of interest (white box). Visual representation of increased variance measured by number and brightness (middle), colour scale represented in quantification graph (right). Quantification of variance (right) across the border from nucleoplasm to nucleolus (example line drawn in middle). Dotted line represents approximate nuclear boundary. **d**–**g**, Image, variance map, and quantified variance of HP4 in S2 cells (**d**), HP5 in S2 cells (**e**), HP1γ in mammalian NIH3T3 cells (**f**), and HP1c in S2 cells (**g**). **h**, Diffusion rate (*D*) for fibrillarin across the nucleoplasm–nucleolus boundary (left), and HP4 (middle) and HP5 (right) across the euchromatin–heterochromatin boundary. For **c**–**h**, $n = 25$ nuclei, error bars are s.d. **i**, Representative image, variance map, and quantified variance across boundary for HP4 in control cells (bw RNAi, top), HP1a-depleted cells (HP1a RNAi, middle),

and HP1a-depleted and rescued cells (HP1a RNAi + mCherry–HP1a, bottom). $n = 25$ nuclei per condition, error bars are s.d. **j**, Predictions of inert probe variance and diffusion near 'H2A edges', which have a >2 fold increase in H2A density (purple bar) with <1.25 fold change in HP1a density (green bar), and 'HP1a edges', which have >3 fold increase in HP1a density (green bar) with <1.25 fold change in H2A density (purple bar). The chromatin compaction model (left) predicts that inert probe variance and diffusion rate would be influenced by increasing H2A density, but unaffected by HP1a density. The phase-separation model (right) predicts that inert probe variance and diffusion rate would be influenced by HP1a density, but unaffected by H2A density. **k**, Summary of RICS and N&B data. Heterochromatin proteins can move freely in the heterochromatin domain (i) but are hindered near the hetero-euchromatic border (ii). Similarly, euchromatic proteins move freely in euchromatin (iii) but are hindered near the border (iv), mostly preventing their entry. Euchromatic proteins that do enter heterochromatin move more slowly owing to energetically costly interactions with surrounding phase particles (v) or crowded environments (vi). **l**, Models of how liquid properties could influence heterochromatin domain formation and functions. We speculate that nucleation of heterochromatic (HP1) foci could occur independently of chromatin and H3K9me2/3, then associate with the chromatin fibre (top left), or nucleation could require H3K9me2/3 (top right). Heterochromatin could spread along the chromatin fibre (in *cis*) due to HP1 liquid 'wetting', followed by H3K9 HMTase recruitment and H3K9 methylation ('HP1 first'), or as previously proposed, HP1 recruitment of the HMTase could result in H3K9 methylation of adjacent nucleosomes, followed by HP1 binding (H3K9me2/3 first). Finally, non-contiguous segments of chromatin (on the same or different chromosomes) can coalesce into one 3D domain, owing to liquid-like fusion events between H3K9me2/3–HP1-enriched regions.